This is the post-print (i.e. final draft post-refereeing) of the publication.
The final publication is available at Elsevier via http://dx.doi.org/10.1016/j.jeurceramsoc.2014.08.033

Improving the functional properties of $(K_{0.5}Na_{0.5})NbO_3$ piezoceramics by acceptor doping

X.Vendrell[1*], J.E. García[2], X.Bril[3], D.A. Ochoa[2], L.Mestres[1], G.Dezanneau[3]

[1]*Departament de Química Inorgànica, Universitat de Barcelona, 08028 Barcelona, Spain*
[2]*Department of Applied Physics, Universitat Politècnica de Catalunya, 08034 Barcelona, Spain*
[3] *Lab. SPMS, Ecole Centrale Paris, Grande voie des vignes 92295 Chatenay-Malabry Cedex, France*

Abstract

ZrO_2 and TiO_2 modified lead-free $(K_{0.5}Na_{0.5})NbO_3$ (KNN) piezoelectric ceramics are prepared by conventional solid-state reaction. The effect of acceptor doping on structural and functional properties are investigated. A decrease in the Curie temperature and an increase in the dielectric constant values are observed when doping. More interestingly, an increase in the coercive field E_c and remanent polarization P_r is observed. The piezoelectric properties are greatly increased when doping with small concentrations dopants. ZrO_2 doped ceramic exhibits good piezoelectric properties with piezoelectric coefficient d_{33}=134 pC/N and electromechanical coupling factor k_p=35%. It is verified that nonlinearity is significantly reduced. Thus, the creation of complex defects capable of pinning the domain wall motion is enhanced with doping, probably due to by the formation of oxygen vacancies. These results strongly suggest that compositional engineering using low concentrations of acceptor doping is a good means of improving the functional properties of KNN lead-free piezoceramic system.

Keywords: Lead-free piezoceramics, Acceptor doping, Piezoelectric properties, $(K,Na)NbO_3$

*Dr. Xavier Vendrell
xavier.vendrell@ub.edu
Telf: +34 934 021 270
Fax: +34 934 907 725

1. Introduction

The most widely used piezoelectric ceramics are $Pb(Ti,Zr)O_3$ (PZT)-based materials, on account of their high piezoelectric response, large-scale production capability and the tailoring of their properties through composition. Due to the high toxicity of lead, a wide range of strict regulations concerning environmental preservation are increasingly being introduced worldwide. Many governments have therefore established legislation regarding waste electric equipment (WEEE), restrictions on hazardous substances (RoHS), and end-of-life vehicles (ELV) to introduce directives regarding environmental pollutants[1]. The search for alternative lead-free piezoelectric materials is currently focused on modified bismuth titanates, alkaline niobates (KNN) and other systems in which a morphotropic phase boundary (MPB) occurs[2–4].

Among the available lead-free piezoelectric materials under study, much attention has been paid over the last few years to $K_{0.5}Na_{0.5}NbO_3$ (KNN)-based ceramics as a result of the breakthrough made by Saito et al.,[5] who obtained high d_{33} (~400pC/N) in the Li-Ta-Sb modified KNN. However, the major drawback of KNN ceramics is the need for special handling of the starting powders, sensitivity of properties to nonstoichiometry, and especially a complex densification process[6]. As regards PZT, sintering aids such CuO, SnO_2, ZnO or MnO_2 may improve sinterability and modify the dielectric and piezoelectric behaviour of the KNN materials[7–11].

Compositional modification by doping is a very active research line for obtaining piezoceramics with enhanced properties. The $(K,Na)NbO_3$-$LiTaO_3$-$LiSbO_3$, particularly the composition $(K_{0.44}Na_{0.52}Li_{0.04})(Nb_{0.86}Ta_{0.10}Sb_{0.04})O_3$, is probably the most workable lead-free piezoelectric system known to date. However, its properties are not suitable for all end use, e.g. for power devices where piezoceramics with low losses and stable properties are required. In this perspective, good results are expected by means of hardener substitutions, such as those that occur in other perovskites[12], although some structural and electrical aspects remain controversial as regards the role of dopants in the KNN system. It has recently been shown that Cu-doped KNN-modified compounds may exhibit typical characteristics of hard behaviour[13–16]. Hardener ions in a perovskite compound (e.g. Cu^{2+}

ions replace Nb^{5+} ions in Cu-doped KNN) are most often acceptors, the introduction of which leads to the creation of oxygen vacancies, thereby forming the so-called complex defects[17]. These defects operate as pinning centres by hampering the motion of the domain walls. This domain wall pinning effect is responsible for the reduction in dielectric losses and stabilization of properties in ferroelectrics[18]. The goal of this study is thus to test the influence of Zr^{4+} and Ti^{4+} acceptor-doping in $(K_{0.5}Na_{0.5})NbO_3$ on the structural, dielectric, piezoelectric and nonlinear properties. The addition of ZrO_2 and TiO_2 is expected to improve functional properties of KNN ceramics for power application, i.e. reduce the losses and increase the properties stability.

2. Experimental

The $(K_{0.5}Na_{0.5})(Nb_{1-x}M_x)O_{3-\square}$ compositions with x = 0.0 and 0.005 being M=Zr or Ti, hereafter abbreviated as KNN-M, were synthesized by conventional solid-state reaction. The raw materials of analytical grade used in this study were K_2CO_3 (99%), Na_2CO_3 (99.5%), Nb_2O_5 (99.9%), ZrO_2 (99%) and TiO_2 (99%). After separate milling, the powders were weighed and mixed by ball milling using ZrO_2 balls in absolute ethanol medium for 3 h, then dried and calcined twice at 700 ºC for 2 h. The calcined powders were then milled again and cold-isostatically pressed at 750 MPa into 7 mm diameter pellets and sintered in air, without a binder, at 1125 ºC for 2 h. Care was taken to ensure that a high alkaline element pressure is maintained during the process by surrounding the pellets with powder of the same composition, and the pellets were deposited on Pt foils to avoid reaction with alumina boats. All as-sintered ceramics showed relative densities over 95% measured by Archimedes' method.

X-ray diffractograms were recorded at room temperature (RT) on a Bruker D2 PHASER equipped with a XFlash detector. A two-axis diffractometer in Bragg-Brentano geometry with Cu $K\alpha_{1,2}$ radiation was used for the *in situ* XRD characterization. The control of temperature was provided by a furnace from 30 ºC to 500 ºC. The cell parameters and their evolution with temperature were refined by a LeBail fitting procedure as implemented in the Fullprof suite[19]. The Raman scattering spectra were obtained on a Labram (Horiba) spectrometer with a He-Ne excitation wavelength of 632.8 nm,

coupled to a Linkam sample holder, with variable temperature from 30 ºC to 500 ºC. DSC measurements were performed on a Seiko apparatus covering the 100 - 1000 K temperature range. Microstructure was evaluated on polished and thermally etched samples (1000 ºC for 5 min for pure KNN and 980 ºC for 5 min for doped KNN) using a Field Emission Scanning Electroc Microscope, FE-SEM (JEOL JSM-7001F). The micrographs were performed on the polished and thermally etched surfaces of the samples coated with graphite. The voltage conditions were set at 20 kV and the work distance was established at 12 mm. In order to analyze the composition of the material, an energy dispersive spectroscopy (EDS) analysis was performed using an OXFORD X-Max^N EDS detector provided with INCA Energy software. A pure Co sample was used as a reference material. The average grain size was determined from the SEM images using an image processing and analysis software (ImageJ). The grain size was expressed as Feret's diameter using more than 400 grains in each measurement. Electrical characterization was carried out on ceramic discs with sputtered gold-chromium electrodes on both parallel surfaces. The temperature dependence of the dielectric permittivity was measured on unpoled samples using an impedance analyzer (HP 4192A) in a frequency range of 100 Hz to 1 MHz and the temperature range of 30 ºC to 600 ºC. The measurements were done during the heating ramp at a rate of 2 ºC/min. The permittivity dependence with a sub-switching ac electric field was measured at 1 kHz and at RT, by means of a capacitance. The hysteresis cycles were recorded using a modified Sawyer-Tower circuit, at 1Hz and at RT. The samples were poled in silicon oil at 80 ºC for 30 minutes under a 30 kV/cm DC electric field. Subsequently, the longitudinal piezoelectric coefficient was measured using a piezo-d_{33} meter (YE2730A, APC International) at RT. The piezoelectric constant d_{31} and the electromechanical coupling factor k_p were determined at RT by the resonance/antiresonance method on the basis of the IEEE standards.

3. Results and discussion

Figure 1(a) shows the XRD patterns of the pure KNN and KNN-M ceramics measured at RT. For all ceramics, a pure perovskite phase indexed in the *Amm2* orthorhombic space group is observed. In contrast to the results obtained by Ramajo et al. [20], no parasitic phases are observed at low

concentration of dopant. Our results suggest that taking special care of the reagents and of the synthesis method plays an important role to avoid the formation of parasitic phases. The cell parameters vary by less than 0.5 %, indicating that the structure does not change significantly upon doping with ZrO_2 or TiO_2. Since the Ti^{4+} and Zr^{4+} ionic radii, 0.61 Å and 0.72 Å, respectively, in a six-fold environment[21], are close to that of Nb^{5+} ion (0.64 Å), dopant atoms should essentially locate on the B-site, which by charge compensation gives rise to the creation of oxygen vacancies. The Raman spectra of the sintered samples (Figure 1(b)) present the typical vibrations corresponding to a perovskite phase, associated with the BO_6 octahedra[22]. No extra signals are detected; thus, no parasitic phases are observed, as confirmed by XRD. The vibrations of the BO_6, A_{1g} (ν_1) and F_{2g} (ν_5) are relatively strong scatterings in systems similar to KNN, because of a near-perfect equilateral octahedral symmetry. Furthermore, the stretching modes (ν_1, ν_5) shift to lower frequencies. This effect may be attributed to a weakening of the bond strength, probably caused by the oxygen vacancies.

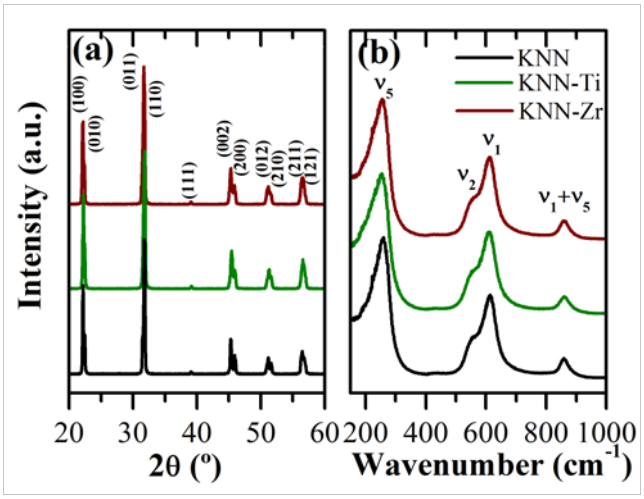

Figure 1: XRD patterns (a) and Raman spectra (b) of the pure KNN and KNN-M ceramics measured at room temperature.

The transition temperatures from orthorhombic to tetragonal phase and from tetragonal to cubic phase are observed at around 200 and 420 ºC, respectively, in pure KNN ceramics [23]. These transitions are confirmed here by different techniques. The analysis of temperature-dependent Raman spectra, XRD patterns and DSC data allows the two transitions for KNN and KNN-M ceramics to be

identified without ambiguity, as shown in Figure 2. All techniques show practically the same transitions temperatures, although the DSC data show lower transition temperatures due to the dynamic acquisition process. When adding 0.5 % of Ti^{4+} and Zr^{4+}-ions on KNN B-site, we observe a decrease of the cubic-to-tetragonal transition temperature of 45 and 25 K, respectively, which is similar to what was previously found in acceptor-doped KNN [24–26]. The tetragonal to orthorhombic temperature transitions decrease only slightly, this effect being higher when doping with TiO_2.

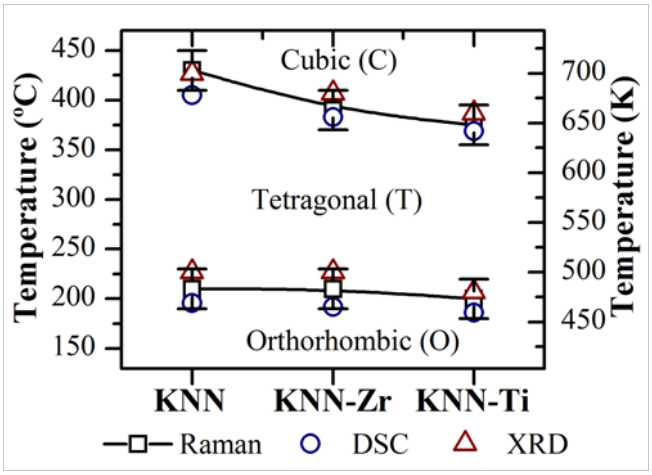

Figure 2: Temperature-composition evolution of the pure KNN and KNN-M ceramics, based on DSC, Raman spectroscopy and XRD measured from 30ºC to 500ºC.

The variation of the microstructures and the grain size distributions of the KNN and KNN-M ceramics is shown in Figure 3 (a)-(f). All the samples exhibit the typical morphology of the alkaline niobate ceramics. Although the pure KNN ceramic micrograph is over-etched, the surface reveals a bimodal microstructure with cube-shape grains ranging from about 500 nm to a few micrometers, with an average grain size of ~3.9 ± 2.3 μm (Figure 3(a,d)). The micrograph and the grain size distributions of the pure KNN also show the presence of some large abnormal grains. When doping with Zr^{4+} or Ti^{4+} ceramics show a decrease of the grain size and an increase of the grain size distribution uniformity, Figures 3(b,e) and (c,f). The average grain size of the KNN-Zr ceramics is ~2.1 ± 1.2 μm, and for the KNN-Ti ceramics is slightly lower ~1.7 ± 1.1 μm. As can be observed in Figures 3(d,e,f) the grain size distributions shifts toward smaller grain sizes when doping and causes the grain size distribution

to become much narrower. Therefore, the addition of acceptor dopants inhibits both the grain growth and the formation of abnormally grown grains, as already observed [20,27]. The limited grain growth observed when doping could be related with a non-uniform distribution of the Zr^{4+} or Ti^{4+} dopants between the grain and the grain boundary. Higher concentration of the dopant in the grain boundary region could hinder the grain growth, as observed for doped $BaTiO_3$ ceramics [28,29]. The TEM studies presented by Malic et al. confirmed the presence of ZrO_2 inclusions boundary region [30] that could avoid the grain growth. In our case, there is also a decrease in the grain growth when doping, although the presence of ZrO_2 inclusions could not be observed in our case. Probably, it can be attributed to the different synthesis method used by Malic et al. were the dopants are added in the powder mixture after the solid state synthesis, thus, in our case the dopants are incorporated in the lattice instead of forming inclusions in the boundary region.

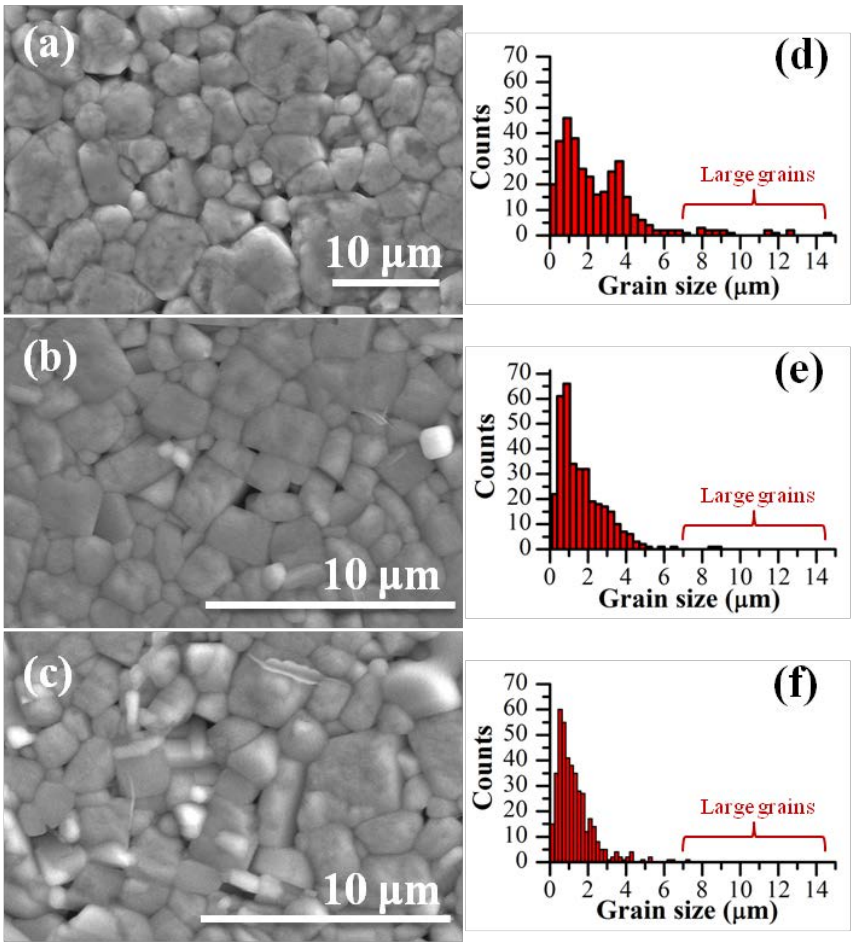

Figure 3: Microstructure and grain size distributions of polished and thermally etched surfaces of pure KNN (a,d), KNN-Zr (b,e) and KNN-Ti (c,f).

No evidence of secondary phases was observed by BSE or EDS analysis, as confirmed by XRD and Raman spectroscopy. The EDS analysis of the matrix reveals that the atomic percentages of elements do not differ significantly from the nominal composition, as reported in Table I. It should be noted that Zr and Ti elements could not be detected due to the low content of dopants. Finally, the matrix grains present a Na/K ratio around 1, which is close to the nominal composition, confirming that the low synthesis temperature and the special care taken when sintering avoid the evaporation of Na or K elements.

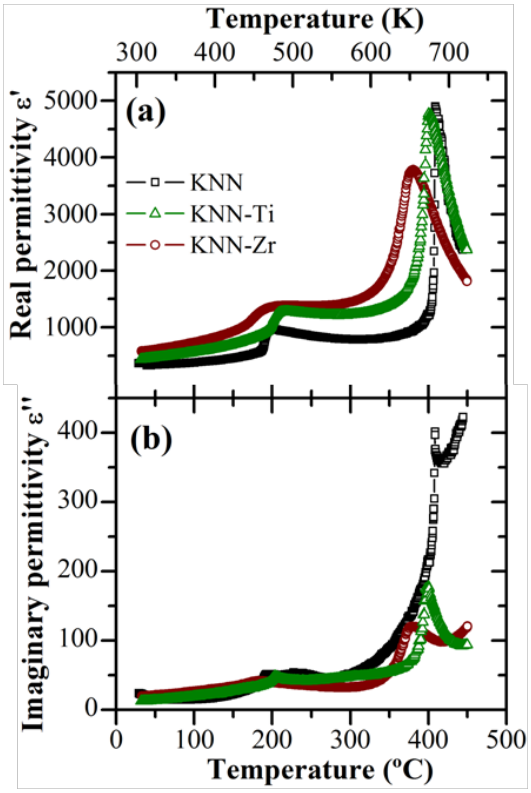

Figure 4: Temperature dependence of the real (a) and imaginary (b) parts of the relative permittivity of pure KNN and KNN-M ceramics sintered at 1125 ºC for 2 h (at 10 kHz).

Table I: Elemental composition of KNN and KNN-M ceramics determined by EDS analysis. This table represents the atomic percentages of elements.

	Na	**K**	**Nb**	**M**	**Na/K**
KNN	10.18±0.32	10.24±0.41	20.44±0.27	-	0.99
KNN-Ti	10.04±0.18	9.98±0.34	20.12±0.16	-	1.01
KNN-Zr	10.09±0.34	10.18±0.27	20.34±0.21	-	0.99
$KNN_{Nominal\ Composition}$	10	10	20	-	1

Figure 4 shows the temperature dependence of the real and imaginary parts of the relative permittivity of pure KNN and KNN-M ceramics, measured at 10 kHz from RT to 450 ºC. Permittivity versus temperature shows two anomalies, one at around 200 ºC associated with the orthorhombic to tetragonal phase transition, and the other at higher temperatures, at which a clear maximum of the permittivity is shown for all ceramics and is associated with the tetragonal ferroelectric to cubic paraelectric phase transition. In doped samples, the orthorhombic-to-tetragonal (*O*-*T*) phase transition shifts slightly toward lower temperatures, while the decrease in temperature of the tetragonal-to-cubic (*T*-*C*) phase transition is much more significant. The temperature change of *O*-*T* and *T*-*C* phase transitions for TiO_2 or ZrO_2 doped samples may also be attributed to the acceptor doping effect [24,30].

As already shown in Figure 4, for pure KNN a typical normal ferroelectric to paraelectric phase transitions is observed showing a narrow phase transition. Meanwhile, the ferroelectric to paraelectric phase transitions broadens on doping, suggesting the appearance of diffuse phase transition. This behaviour may be induced in many ways, such as by microscopic compositional fluctuation, by the merging of micro-domains into macro-domains, or via a coupling of the order parameter and local disorder mode through local strain [31]. The diffuse phase transition is observed for both TiO_2 and ZrO_2 doped KNN ceramics. Thus, one probable cause of this behaviour is local fluctuations induced by the incorporation of Ti^{4+} or Zr^{4+} ions, whose valence is different from the Nb^{5+} one, into the crystalline lattice of the perovskite.

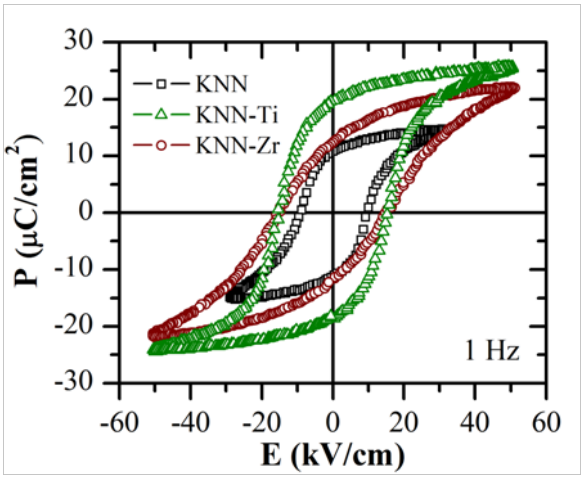

Figure 5: P-E hysteresis loops of the pure KNN and KNN-M ceramics measured at room temperature and at 1 Hz.

Table II: Properties of pure KNN and KNN-M ceramics at room temperature.

	$\rho_{relative}$ (%)	ε' (10 kHz)	tanδ (10 kHz)	(-)d_{31} (pC/N)	k_p (%)	d_{33} (pC/N)	α (10^{-3} mV^{-1})
KNN	95.1±0.4	338	0.061	19	28	96	0.452
KNN-Ti	97.4±0.2	510	0.032	35	33	124	0.385
KNN-Zr	98.2±0.2	402	0.036	37	35	134	0.323

Polarization versus electric field, (P-E) hysteresis loops for pure and doped KNN ceramics measured at 1Hz and at RT are shown in Figure 5. Only KNN ceramic possesses well-saturated *P-E* loop under an electric field of 30 kV/cm. A higher electric field must therefore be applied to doped KNN ceramics to obtain a well-saturated hysteresis loop. The coercive field E_c and the remanent polarization P_r of pure KNN are 8.5 kV/cm and 11.4 μC/cm^2 , respectively. These two values increase with doping. The increase in E_c means that the material becomes harder, which is consistent with the assumption that oxygen vacancies are formed, and the so-called complex defects are produced by these acceptors additives. However, P_r shows an increase when doping with ZrO_2 up to 19.8 μC/cm^2 and an increase to 12.4 μC/cm^2 when adding TiO_2. This fact can be explained taking into account that the density of the material is enhanced by doping, as is reported in Table II. The piezoelectric properties are also improved, as shown in Table II. The d_{33} value for the undoped KNN is 96 pC/N, which is close to that reported by Guo *et al.* [32]. The d_{33} and k_p are significantly enhanced when doping with TiO_2 and ZrO_2, reaching higher values of the two coefficients reported by other authors when doping with a higher concentration of acceptor dopants [33]. KNN-M ceramics also show an improvement in dielectric properties at RT. Results point out that low amounts of acceptor dopants promote the densification; thus, enhanced remanent polarization, piezoelectric coefficient and dielectric constant are obtained in KNN-M ceramics. The lower values of relative permittivity and the higher dielectric losses observed for the pure KNN ceramic could be related with its lower density, but a slight deficiency of alkaline metals could not be discarded since the functional properties of the ceramics strongly depends on the stoichiometry [34]. Although in our case, as observed by EDS analysis, the ratio Na/K is close to 1. Moreover, as observed in $BaTiO_3$-based ceramics [35], the relative permittivity increases when the grain size decreases, reaching a maximum of permittivity at ~

1 µm. Therefore, in our case, the increase of the relative permittivity can be attributed not only to the slight increase of the relative density, but also to the decrease of the grain size when doping.

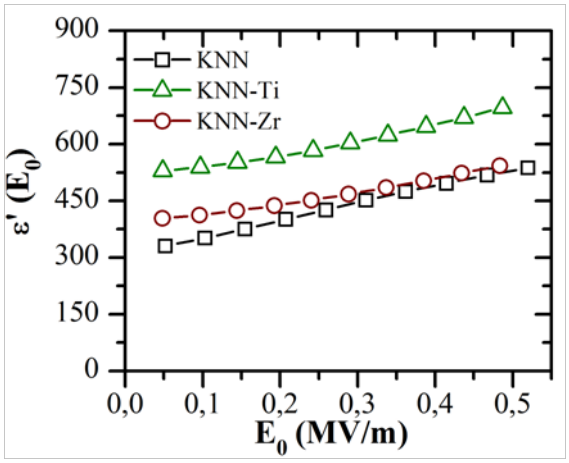

Figure 6: Dielectric constant as a function of the electric field amplitude of the pure KNN and KNN-M ceramics, measured at 1 kHz and at room temperature.

The dielectric and piezoelectric responses of piezoelectric materials are nonlinear under a high electric field. This nonlinear behaviour is satisfactorily described by the Rayleigh model on PZT [36,37] and KNN-based [38–40] ceramics. The nonlinear dielectric and piezoelectric behaviour is principally caused by the irreversible movement of the ferroelectric domain walls. The Rayleigh relation $\varepsilon'(E_0)=\varepsilon'(0)+\alpha E_0$ is typically used in order to analyse the nonlinear dielectric response, E_0 being the amplitude of the electric field, α the Rayleigh coefficient, $\varepsilon'(0)$ the relative permittivity at very low E_0, and $\varepsilon'(E_0)$ the measured relative permittivity as a function of the electric field amplitude E_0. The slope α of the $\Delta\varepsilon'$ ($\Delta\varepsilon'=\varepsilon'(E_0)-\varepsilon'(0)$) versus E_0 plot is used to evaluate the nonlinearity numerically; therefore, the higher the Rayleigh coefficient the higher the instability of the dielectric response. Figure 6 shows ε' versus E_0 plot for pure KNN and KNN-M ceramics. A linear relation is verified for all samples, as predicted by the Rayleigh model. Rayleigh coefficients are calculated and reported in Table II. As one may observe, KNN-M ceramics show better stability than pure KNN. Consequently, acceptor dopants may lead to the formation of oxygen vacancies, and thereby facilitate the creation of the complex defects that may act by hampering the domain wall motion.

4. Conclusions

Oxygen vacancies are induced by introducing Ti^{4+} or Zr^{4+} ions into the B-site of the KNN perovskite, which is prepared by conventional solid-state reaction. The addition of TiO_2 or ZrO_2 shifts the phase transitions toward lower temperatures, as confirmed by different techniques, this effect being higher when doping with TiO_2. The addition of low amounts of acceptor dopants promotes the densification, improving functional properties of KNN ceramics. The piezoelectric properties of the ceramics are greatly enhanced when doping with small concentrations of TiO_2 or ZrO_2. The coercive field increases and the dielectric losses decrease when KNN is doped, which is consistent with the hypothesis that oxygen vacancies are formed by acceptor doping. Acceptor-doped KNN piezoceramics exhibit an increase in the stability of the properties (nonlinear behaviour reduction) probably as a consequence of the domain wall pinning effect. Therefore, doping with low amounts of acceptor dopants should be taken into consideration in order to improve the functional properties of KNN-based piezoceramics, i.e. an increase of the dielectric constant, the piezoelectric coefficients, and the coupling factor as well as a decrease of the losses and the instability of the properties.

Acknowledgements

The authors would like to thank the Spanish Government MAT2010-21088-C03 Project, the Catalan Government PIGC project 2009-SGR-0674 and the French Agence Nationale de la Recherche, *Surffer* project, for their financial support.

References

[1] EU-Directive 2002/95/EC: Restriction of the use of certain hazardous substances in electrical and electronic equipment (RoHS). Off J Eur Union 2003;46:19.

[2] Maeda T, Hemsel T, Morita T. Piezoelectric Properties of Li-Doped (K0.48Na0.52)NbO3 Ceramics Synthesized Using Hydrothermally-Derived KNbO3 and NaNbO3 Fine Powders. Jpn J Appl Phys 2012;51:1–4.

[3] Zhang S, Xia R, Shrout TR. Modified (K[sub 0.5]Na[sub 0.5])NbO[sub 3] based lead-free piezoelectrics with broad temperature usage range. Appl Phys Lett 2007;91:132913.

[4] Rödel J, Jo W, Seifert KTP, Anton E-M, Granzow T, Damjanovic D. Perspective on the Development of Lead-free Piezoceramics. J Am Ceram Soc 2009;92:1153–77.

[5] Saito Y, Takao H, Tani T, Nonoyama T, Takatori K, Homma T, et al. Lead-free piezoceramics. Nature 2004;432:84.

[6] Kosec M, Kolar D. On activated sintering and electrical properties of NaKNbO3. Mater Res Bull 1975;10:335–9.

[7] Lin D, Kwok KW, Chan HLW. Piezoelectric and ferroelectric properties of Cu-doped K 0.5 Na 0.5 NbO 3 lead-free ceramics. J Phys D Appl Phys 2008;41:045401.

[8] Saeri MR, Barzegar A, Ahmadi Moghadam H. Investigation of nano particle additives on lithium doped KNN lead free piezoelectric ceramics. Ceram Int 2011;37:3083–7.

[9] Li Z, Xu G, Li Y, Sun A, Duan L, Jiang J, et al. Dielectric and piezoelectric properties of ZnO and SnO2 co-doping K0.5Na0.5Nbo3 ceramics. Phys B Condens Matter 2010;405:296–9.

[10] Kang I-Y, Seo I-T, Cha Y-J, Choi J-H, Nahm S, Sung T-H, et al. Low temperature sintering of ZnO and MnO2-added (Na0.5K0.5)NbO3 ceramics. J Eur Ceram Soc 2012;32:2381–7.

[11] Rubio-Marcos F, Romero JJ, Navarro-Rojero MG, Fernandez JF. Effect of ZnO on the structure, microstructure and electrical properties of KNN-modified piezoceramics. J Eur Ceram Soc 2009;29:3045–52.

[12] Jaffe B, Cook WR, Jaffe H. Piezoelectric ceramics. Academic Press: London, New York; 1971.

[13] Matsubara M, Yamaguchi T, Sakamoto W, Kikuta K, Yogo T, Hirano S. Processing and Piezoelectric Properties of Lead-Free (K,Na) (Nb,Ta) O3 Ceramics. J Am Ceram Soc 2005;88:1190–6.

[14] Lin D, Kwok KW, Chan HLW. Structure, dielectric, and piezoelectric properties of CuO-doped K[sub 0.5]Na[sub 0.5]NbO[sub 3]–BaTiO[sub 3] lead-free ceramics. J Appl Phys 2007;102:074113.

[15] Zhang S, Lim JB, Lee HJ, Shrout TR. Characterization of hard piezoelectric lead-free ceramics. IEEE Trans Ultrason Ferroelectr Freq Control 2009;56:1523–7.

[16] Lim JB, Zhang S, Jeon J-H, Shrout TR. (K,Na)NbO 3 -Based Ceramics for Piezoelectric “Hard”Lead-Free Materials. J Am Ceram Soc 2010;1220:2009–11.

[17] Takahashi S. Effects of impurity doping in lead zirconate-titanate ceramics. Ferroelectrics 1982;41:143–56.

[18] Albareda A, Pérez R, García JE, Ochoa DA, Gomis V, Eiras JA. Influence of donor and acceptor substitutions on the extrinsic behaviour of PZT piezoceramics. J Eur Ceram Soc 2007;27:4025–8.

[19] Rodriguez-Carvajal J. Recent advances in magnetic structure determination by neutron powder diffraction. Phys B Condens Matter 1993;192:55.

[20] Ramajo L, Taub J, Castro MS. Influence of zirconium addition on final properties of K0.5Na0.5NbO3-based ceramics. J Mater Sci Mater Electron 2013;25:168–73.

[21] Shannon RD. Revised Effective Ionic Radii and Systematic Studies of Interatomie Distances in Halides and Chaleogenides. Acta Crystallogr 1976;A32:751–67.

[22] Kakimoto K, Akao K, Guo Y, Ohsato H. Raman Scattering Study of Piezoelectric (Na 0.5 K 0.5)NbO 3 -LiNbO 3 Ceramics. Jpn J Appl Phys 2005;44:7064–7.

[23] Tellier J, Malic B, Dkhil B, Jenko D, Cilensek J, Kosec M. Crystal structure and phase transitions of sodium potassium niobate perovskites. Solid State Sci 2009;11:320–4.

[24] Lee Y, Yoo J, Lee K, Kim I, Song J, Park Y-W. Dielectric and piezoelectric characteristics of the non-stoichiometric (Na,K)NbO3 ceramics doped with CuO. J Alloys Compd 2010;506:872–6.

[25] Zuo R, Rodel J, Chen R, Li L. Sintering and Electrical Properties of Lead-Free Na0.5K0.5NbO3 Piezoelectric Ceramics. J Am Ceram Soc 2006;89:2010–5.

[26] Pang X, Qiu J, Zhu K, Du J. Effect of ZnO on the microstructure and electrical properties of (K0.5Na0.5)NbO3 lead-free piezoelectric ceramics. J Mater Sci Mater Electron 2011;23:1083–6.

[27] Wang X, Wu J, Cheng X, Zhang B, Zhu J, Xiao D. Compositional dependence of phase structure and electrical properties in (K0.50Na0.50)0.97Bi0.01(Nb1−xZrx)O3 lead-free ceramics. Ceram Int 2013;39:8021–4.

[28] Urek S, Drofenik M, Makovec D. Sintering and properties of highly donor-doped barium titanate ceramics. J Mater Sci 2000;5:895–901.

[29] Park JS, Han YH. Effects of MgO coating on microstructure and dielectric properties of BaTiO3. J Eur Ceram Soc 2007;27:1077–82.

[30] Malic B, Bernard J, Bencan A, Kosec M. Influence of zirconia addition on the microstructure of K0.5Na0.5NbO3 ceramics. J Eur Ceram Soc 2008;28:1191–6.

[31] Rubio-Marcos F, Marchet P, Merle-Méjean T, Fernandez JF. Role of sintering time, crystalline phases and symmetry in the piezoelectric properties of lead-free KNN-modified ceramics. Mater Chem Phys 2010;123:91–7.

[32] Guo Y, Kakimoto K, Ohsato H. Phase transitional behavior and piezoelectric properties of (Na[sub 0.5]K[sub 0.5])NbO[sub 3]–LiNbO[sub 3] ceramics. Appl Phys Lett 2004;85:4121.

[33] Zang G-Z, Yi X-J, Du J, Wang Y-F. Co2O3 doped (Na0.65K0.35)NbO3 piezoceramics. Mater Lett 2010;64:1394–7.

[34] Lee Y, Cho J, Kim B, Choi D. Piezoelectric Properties and Densification Based on Control of Volatile Mass of Potassium and Sodium in (K 0.5 Na 0.5)NbO 3 Ceramics. Jpn J Appl Phys 2008;47:4620–2.

[35] Arlt G, Hennings D, With G. Dielectric properties of fine-grained barium titanate ceramics. J Ap 1985;58:1619–25.

[36] García JE, Pérez R, Ochoa DA, Albareda A, Lente MH, Eiras JA. Evaluation of domain wall motion in lead zirconate titanate ceramics by nonlinear response measurements. J Appl Phys 2008;103:054108.

[37] Pramanick A, Damjanovic D, Nino JC, Jones JL. Subcoercive Cyclic Electrical Loading of Lead Zirconate Titanate Ceramics I: Nonlinearities and Losses in the Converse Piezoelectric Effect. J Am Ceram Soc 2009;92:2291–9.

[38] Ochoa DA, García JE, Pérez R, Gomis V, Albareda A, Rubio-Marcos F, et al. Extrinsic contribution and non-linear response in lead-free KNN-modified piezoceramics. J Phys D Appl Phys 2009;42:025402.

[39] Vendrell X, García JE, Rubio-Marcos F, Ochoa DA, Mestres L, Fernández JF. Exploring different sintering atmospheres to reduce nonlinear response of modified KNN piezoceramics. J Eur Ceram Soc 2013;33:825–31.

[40] Peng B, Yue Z, Li L. Evaluation of domain wall motion during polymorphic phase transition in (K,Na)NbO3-based piezoelectric ceramics by nonlinear response measurements. J Appl Phys 2011;109:054107.